JOURNAL OF GEOPHYSICAL RESEARCH, VOL. 105, NO. A1, PAGES 47–60, JANUARY 1, 2000

Influence of Coulomb collisions on isotopic and elemental fractionation in the solar wind acceleration process

Roland Bodmer
Physikalisches Institut, University of Bern, Bern, Switzerland, and
Max-Planck-Institut für Aeronomie, Katlenburg-Lindau, Germany

Peter Bochsler
Physikalisches Institut, University of Bern, Bern, Switzerland

Abstract. In view of new observational evidence from isotope spectrometers on WIND, SOHO (Solar Heliospheric Observatory), and ACE (Advanced Composition Explorer), we explore the efficiency of isotope fractionation processes in the inner corona. We reinvestigate the role of Coulomb collisions in the acceleration of minor ions using a multifluid model. To model the main gas, we study stationary solutions for the continuity and momentum equations of electrons, protons, and alpha particles. As a closure of the system of equations, we prescribe expansion geometry and temperature profiles based on observations. The behavior of minor ions, which are treated as test particles, depends in a complicated manner on their mass and on their charge, structured by the interplay of acceleration, gravity, pressure gradient, electromagnetic fields, Coulomb drag, and thermal diffusion. We compare the fractionation effects in different solar wind regimes: In our model high-speed solar wind emanating from polar coronal holes, Coulomb friction practically equalizes the velocities of all species, and no substantial fractionation takes place. In the case of a rapidly expanding magnetic field geometry, for example, in the vicinity of a coronal streamer, the proton flux and thus the Coulomb friction on minor ions is reduced, leading to depletion of heavy species in the solar wind. The model also predicts a substantial depletion of alpha particles relative to protons in the heliospheric current sheet, consistent with observations. In such a situation, heavy elements are depleted in the solar wind relative to protons as well, but the effect is strongest for alpha particles. Isotopic fractionation of helium of the order of 30% is possible, while the isotope effect on heavier elements amounts at most to a few percent per mass unit.

1. Introduction

Knowledge about the elemental and isotopic composition of the Sun is a crucial ingredient for the understanding of the genesis and evolution of the solar system because the Sun comprises more than 99% of the total mass of the solar system. From spectroscopic analysis of photospheric lines, the abundances of a variety of elements can be determined [*Anders and Grevesse*, 1989]. The solar isotopic composition, however, is difficult to measure accurately by optical spectroscopy because isotopic shifts of atomic lines are much smaller than the corresponding line widths. Usually the solar isotopic composition is inferred in an indirect manner from planetary samples. Direct information on the solar isotopic composition can be derived from the solar wind. The purpose of the present paper is to investigate in a quantitative manner the degree of authenticity of solar wind samples for the composition of the solar atmosphere.

The composition of the solar wind and its relation to the composition of the solar atmosphere has been investigated for three decades by in situ measurements. The instrumentation has undergone a continuous development: With electrostatic analyzers [e.g., *Bame et al.*, 1968] it was possible to identify the most prominent ion species in the solar wind, including the two helium isotopes when the solar wind conditions were favorable. With the foil collection technique used on the Apollo flights [*Geiss et al.*, 1972] it was possible to determine the elemental and isotopic abundances of light solar wind noble gases. These experiments were followed by magnetic mass spectrometers like the Ion Compo-

Paper number 1999JA900434.
0148-0227/00/1999JA900434$09.00

sition Instrument (ICI) on the third International Sun Earth Explorer (ISEE 3) [e.g., *Coplan et al.*, 1984], which could continuously measure mass/charge spectra in the solar wind. The generation of linear time-of-flight mass spectrometers such as Ulysses/SWICS (Solar Wind Ion Composition Spectrometer) [*Gloeckler et al.*, 1992] allowed, furthermore, the unique determination of mass and charge of the dominant solar wind elements. The best mass resolution can be achieved by the new generation of isochronous time-of-flight mass spectrometers, i.e., WIND/MASS [*Gloeckler et al.*, 1995], SOHO/MTOF (Mass Time of Flight) [*Hovestadt et al.*, 1995], and ACE/SWIMS (Solar Wind Ion Mass Spectrometer) [*Gloeckler et al.*, 1998]. With these instruments it is, for the first time, possible to continuously determine the isotopic composition of non-noble gas elements under variable solar wind conditions.

In order to determine the elemental and isotopic composition of the outer convective zone of the Sun from measurements in the solar wind, the relation between the composition of the reservoir and its outflow has to be known. While turbulent mixing causes fairly homogeneous abundances in the convection zone, mixing is reduced above the photosphere, and the decreasing densities and thus decreasing collision frequencies allow differential speeds and abundance variations to arise. The bulk speed of the heavy ions is affected by the acceleration resulting from gravity, pressure gradient, Coulomb drag, thermal diffusion, electromagnetic fields, and wave particle interactions. The differential speeds result from the dependence of the relevant forces on the mass and on the charge of the particle species. As the charge of the ions is altered by ionization and recombination processes, fractionation dependent on elements is also possible in various layers of the solar atmosphere.

Here we focus on the acceleration process of the solar wind and develop a model for the prediction of the magnitude of fractionation effects occurring between the lower corona and the distant solar wind. For lack of a realistic one-dimensional steady state model, we do not consider the transition region and the chromosphere, where a fractionation process dependent on the first ionization potential (FIP) of the particles is known to work [e.g., *Meyer*, 1985]. Models for the FIP effect by *von Steiger and Geiss* [1989], by *Marsch et al.* [1995], and by *Peter* [1996] indicate no significant fractionation of isotopes, even in the case of $^4He/^3He$.

2. Model

2.1. General Description

We develop a multifluid model of the acceleration region of the solar wind with electrons, protons, and alpha particles as main components, while the less abundant elements and isotopes are treated as test species. The conceptual basis of this kind of model was laid by *Geiss et al.* [1970], *Bürgi and Geiss* [1986], *Bürgi* [1992], and *Hansteen and Leer* [1995]. We assume stationary, one-dimensional flow along a magnetic flux tube with a prescribed geometry of superradial expansion. The density and velocity profiles of all species are found by solving the equations of continuity and momentum, while the temperature profiles are prescribed. We use the available free parameters to model two different flow regimes in the solar wind: high-speed solar wind from a polar coronal hole and slow speed solar wind from a coronal streamer. The physical ingredients in our model are essentially the same as given by *Bürgi and Geiss* [1986], with the exception that we prescribe temperature profiles instead of a density profile. This allows us to define a temperature profile for each species separately, and it makes it possible to study the effect of mass-proportional temperatures. More elaborate models exist for the explanation of the behavior of electrons and protons in the solar wind, for example, taking into account anisotropic pressure [e.g., *Hu et al.*, 1997], self-consistent heat fluxes [e.g., *Olsen et al.*, 1998], or distribution functions far from Maxwellians [e.g., *Leblanc and Hubert*, 1997]. We rely on relatively simple equations in order to reduce the number of unknowns and questionable assumptions in the complicated multifluid problem. The new aspect of our work lies mainly in the discussion and interpretation of the results in terms of elemental and isotopic fractionation.

2.2. Flux Tube Geometry

For a one-dimensional description of a multifluid flowing along magnetic field lines, the flux tube cross section $a(r) \propto r^2 f(r)$ has to be prescribed as a function of heliocentric distance r. The superradial expansion factor $f(r)$ is introduced in order to account for nonradial fields. It can be found from the radial component B_r of a given three-dimensional field using magnetic flux conservation:

$$f(r) := \frac{B_r(r_0) r_0^2}{B_r(r) r^2}, \tag{1}$$

where r_0 denotes the solar (photospheric) radius. We use the field geometry from *Wang and Sheeley Jr.* [1990], which is depicted in Figure 1. This magnetic field is current-free everywhere except at the heliospheric current sheet which fills the ecliptic plane outside 2.5 solar radii. The resulting configuration corresponds to solar activity minimum conditions with polar coronal holes and equatorial streamers. In the following we will discuss two models, one representing fast solar wind emanating from coronal holes and one describing slow solar wind close to the coronal streamer.

To model the coronal hole type solar wind, we choose the straight polar field line which originates in the center of the polar coronal hole. The flux tube expands slowly and monotonically over a distance of ~8 solar radii, finally reaching a superradial expansion factor of

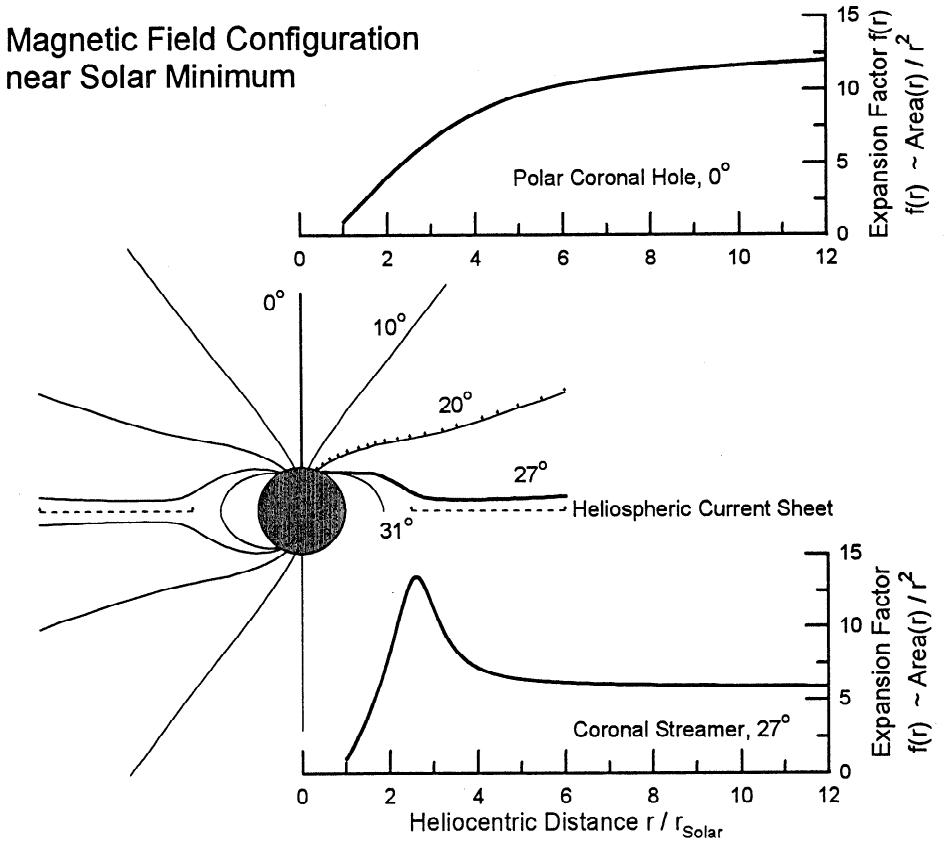

Figure 1. The magnetic field configuration in the corona, adopted from *Wang and Sheeley Jr.* [1990], is representative for the solar activity minimum. The superradial expansion factor is given for the flux tubes originating at a colatitude of 0° (coronal hole) and 27° (coronal streamer).

12. For the slow solar wind above a coronal streamer, however, we use an open field line rooted at a colatitude of 27°, which turns toward lower latitudes and becomes radial close to the heliospheric current sheet. The flux tube expands rapidly between 1 and 2.5 solar radii, where it reaches a local maximum expansion factor of 13, while the overall expansion factor is ~6 only. The superradial expansion factor for the two cases is prescribed using a parametrization introduced by *Bürgi* [1992],

$$f(r) = f_{m1} + \frac{f_1 - f_{m1}}{\exp(\frac{r-r_1}{\sigma_1}) + 1} + \frac{f_{m2}}{1 + (\frac{r-r_2}{\sigma_2})^2}, \qquad (2)$$

where f_{m1} quantifies the overall superradial expansion, which is centered at position r_1 with a width of σ_1. An enhanced local expansion in a region of width σ_2 around r_2 can be obtained by choosing a positive value of f_{m2}. The parameter f_1 is fixed by the condition $f(r_0) = 1$. In Table 1 we give the parameters used to model the expansion geometry for the two solar wind types.

2.3. Continuity Equation

Since a restricted temperature range is considered, only fully ionized hydrogen and helium is included for the main component, while the radial evolution of the charge states is taken into account for test gases. For every particle species x with ionization state j, the number density $n_{x,j}$ and the bulk velocity $\mathbf{v_{x,j}}$ fulfill the continuity equation

$$\frac{\partial n_{x,j}}{\partial t} + \nabla \cdot (n_{x,j}\mathbf{v_{x,j}}) = \qquad (3)$$
$$n_e(J_{j-1}n_{x,j-1} - R_j n_{x,j} - J_j n_{x,j} + R_{j+1}n_{x,j+1}).$$

The term on the right-hand side describes ionization and recombination from and into neighboring charge states induced by electronic collisions. The rate coefficients for ionization (J) and recombination (R), taken from *Arnaud and Rothenflug* [1985], depend on the element, its charge state, and on the electron temperature.

Table 1. Parameters for Expansion Geometry

Parameter	Coronal Streamer	Coronal Hole
f_{m1}	5.89	12.15
r_1	1.400 r_0	-1.53 r_0
σ_1	0.556 r_0	3.77 r_0
f_{m2}	8.51	4.68
r_2	2.570 r_0	3.25 r_0
σ_2	0.629 r_0	4.71 r_0

Here $r_0 \equiv$ solar radius.

Summation of the continuity equations over all charge states of species x and integration in the stationary case leads to

$$n_x(r)v_{xr}(r)r^2 f(r) = \Phi_x(r) = \text{const}, \qquad (4)$$

which describes the conservation of the flux Φ_x of an element or isotope along a flux tube. Here n_x denotes the total density, and v_{xr} denotes the average radial velocity component of all charge states of the species x.

2.4. Momentum Equation

In principle each charge state j of a particle species x has its own velocity field $\mathbf{v_{x,j}}$ and a corresponding momentum equation. However, for the fractionation question, only the weighted average velocity $\mathbf{v_x}$ is of interest. For most elements, there are only a few charge states significantly contributing to the local charge state distribution. Usually, the flow speeds of those charge states are not far from their average due to momentum transfer in ionization/recombination events. Instead of solving a complicated system of coupled momentum equations for the individual speeds and taking the average afterward, we substantially reduce the computational complexity by using an equation for $\mathbf{v_x}$.

Such an equation is found by replacing the individual speeds of the charge states by the average speed $\mathbf{v_x}$ and by summation of the momentum equations over the charge states of species x:

$$\begin{aligned} m_x n_x\left(\frac{\partial \mathbf{v_x}}{\partial t} + (\mathbf{v_x}\cdot\nabla)\mathbf{v_x}\right) &= \mathbf{F_C} + \mathbf{F_W} + \mathbf{F_T} \\ &- \nabla p_x - \frac{GMm_x n_x}{r^2}\mathbf{e_r} + n_x\overline{Z_x}e(\mathbf{E} + \mathbf{v_x}\times\mathbf{B}) \\ &+ m_x n_x(2\mathbf{v_x}\times\boldsymbol{\Omega_0} + \boldsymbol{\Omega_0}\times\mathbf{r}\times\boldsymbol{\Omega_0}), \end{aligned} \qquad (5)$$

where we use the particle mass m_x, its number density n_x, and its partial pressure $p_x = n_x kT_x$, the gravitational constant G, the solar mass M, the electric field $\mathbf{E}$, the magnetic field $\mathbf{B}$, and the heliocentric distance r. The forces caused by collisions with protons and alpha particles are Coulomb friction $\mathbf{F_C}$ [*Geiss et al.*, 1970] and thermal diffusion $\mathbf{F_T}$ [*St.-Maurice and Schunk*, 1976]. We include a wave force $\mathbf{F_W}$ resulting from undamped Alfvén waves propagating away from the Sun [*McKenzie et al.*, 1979]. The corresponding wave energy flux f_W is completely converted into bulk motion without any coronal heating effect. However, we neglect further momentum addition, eventually caused by dissipation of waves (coronal heating).

Below the Alfvénic point at ~10 solar radii, the magnetic tension is strong enough to force the plasma into corotation with the solar surface, while at larger distances, the kinetic energy dominates, and the flow is more and more radial, leading to the well-known Parker spiral magnetic field. We use a frame of reference that corotates with the solar angular velocity $\boldsymbol{\Omega_0}$; therefore Coriolis and centrifugal forces have to be taken into account. Those are the forces that prevent corotation of the plasma at large distances.

The particle charge state used for the electromagnetic forces is $\overline{Z_x}(r)$ which is the average charge state of the element x at the given radial distance. Furthermore, the thermal diffusion force and the Coulomb friction force contain a term proportional to $\overline{Z_x^2}(r)$, which denotes the radial dependence of the average squared charge. We eliminate the equations for electrons by assuming negligible electron mass, charge neutrality, and zero field-aligned current. Instead of solving energy equations containing an ad hoc heating function as has been done by *Hansteen et al.* [1997] and many other authors, we prescribe the temperature profile $T_x(r)$ for each species.

The reduction from three dimensions to one dimension is done assuming rotational symmetry and neglecting components of magnetic fields and velocities in the ϑ direction [*McKenzie et al.*, 1979]. In the frame corotating with the solar surface, all velocities are parallel to the magnetic field. Thus the azimuthal velocity components are proportional to the radial components and can be eliminated using the local magnetic field direction. The continuity equation for particle species x (equation 4) allows us to describe densities in terms of radial velocities v_{xr} if the integral flux Φ_x is a prescribed constant. The radial momentum equation for particle species x then turns into an ordinary differential equation for v_{xr}, and its solution is required to pass through a critical point. The momentum equations for all main gas particles have to be solved simultaneously. We refer to *Bodmer* [1996] for details about the numerical method used to find the solutions.

2.5. Free Parameters

Besides the parameters used for the description of the expansion factor $f(r)$, we have some free parameters available for adapting the model to observations: the particle fluxes Φ_x, the wave action flux, and the temperature profiles $T_x(r)$. The fluxes of the main ions, protons and alpha particles, are chosen according to in situ observations of the solar wind. As the resulting (radial) velocity profiles $v_x(r)$ do not depend on the test gas fluxes, those fluxes do not modify neither the fractionation factors (see (7)) nor the enrichment factors as defined in (8). The test gas fluxes can thus be set to an arbitrary value. The temperature profiles for protons and electrons are sunward extrapolations of the temperatures measured by Helios in the solar wind from 0.3 to 1 AU [*Marsch*, 1991]. From the upper transition region to the lower corona the temperatures were adapted to the plasma temperature from a model by *Gabriel* [1976]. The resulting temperature profiles have a temperature maximum at ~1.13 solar radii. In a first set of models the temperatures of all ions are assumed to be equal to the proton temperature. In section 6 we will discuss the results from an alternative set of models with assumption of mass-proportional temperatures. The remain-

ing free parameter, the wave action flux [*Isenberg and Hollweg*, 1982], determines the amplitude of the Alfvén waves propagating away from the Sun. As the resulting wave force $\mathbf{F_W}$ acts predominantly in the supersonic region, its main effect is to increase the asymptotic speed of the plasma. We thus adjust the wave action flux in each model to obtain a solar wind speed at 1 AU consistent with observations. With this measure, velocity differences among minor species due to inefficient Coulomb friction will transform into differences in densities due to flux conservation and hence to fractionation as discussed in section 3.

3. Fractionation in Stationary Models

The measurement of isotopic abundance ratios in the solar wind is the most direct method to determine isotopic abundances of the outer convective zone of the Sun. The flux ratio of two isotopes in the solar wind, which is independent of radial distance in the stationary case, however, can differ from the density ratio in the convective zone or the photosphere due to fractionation processes. We define the fractionation factor between the isotopes x and y with respect to a reference level at some radial distance r_b as

$$\text{fractionation}(x,y) := \frac{\Phi_x/\Phi_y}{n_x(r_b)/n_y(r_b)}. \qquad (6)$$

Using (4) to evaluate the integral flux constants Φ_x and Φ_y at the position r_b and inserting the results into (6) leads to

$$\text{fractionation}(x,y) = \frac{v_x(r_b)}{v_y(r_b)}. \qquad (7)$$

To model the fractionation with respect to a reference level r_b, the velocity ratio of two isotopes has to be calculated at this level. In a nonstationary model this ratio would remain unchanged if averaged radial velocities were used. In our stationary model the velocity profiles are determined by the momentum equations together with the "boundary" conditions at the critical points which are located in a region between 2 and 8 solar radii. So for a test particle the velocity profile has to be integrated inward from the critical point $r_{c,x}$ until the reference level r_b is reached. The fractionation factor is thus determined by the location of the critical point, the critical velocity $v_{c,x} = v_x(r_{c,x})$, and all the forces acting on the particles between the reference level r_b and the critical point.

The numerical determination of fractionation factors with respect to a reference level $r_b = r_0$ in the photosphere is difficult, since test particles move through a large range of temperatures and densities, and at the base additional processes gain importance, for example, because low charge states of the main gas ions (He^+) have to be taken into account. Our one-dimensional equations are not suited for the description of the complex and nonstationary processes occurring in the chromosphere and in the lower transition zone. Instead we intend to compare the solar wind abundances to coronal abundances at a coronal base level $r_b = 1.2r_0$, whose selection is somewhat arbitrary, but whereon we believe our treatment is more or less appropriate. Our model should then explain differences between coronal base density ratios and solar wind flux ratios.

Resonant waves are known to generate differential streaming of heavy ions and to modify the particle distribution functions. Our model does not include these effects and therefore the behavior of temperatures, velocities, and densities in the far solar wind is not completely consistent with in situ observations. However, processes in the interplanetary space outside the critical points, i.e., in the supersonic region, do not affect the fluxes and have no influence on the fractionation factor defined in (6). Furthermore, in the case of negligible relative speeds in the far solar wind, the fractionation factor given as a ratio of velocities in (7) corresponds to a density (or flux) ratio measured in the solar wind relative to the density ratio at the base.

4. Results

We explore the fractionation of elements and isotopes in two different solar wind regimes as characterized in Table 1: the slow solar wind from a coronal streamer and the high-speed solar wind emanating from the center of a polar coronal hole. The differences between these two models lie in the geometry which results in different superradial expansion factors (see Figure 1), in the temperature profiles which are chosen to fit some observational constraints, in the influence of rotation forces on the low-latitude coronal streamer, and in the energy flux f_W of outward-propagating Alfvén waves entering the flux tube at the solar surface. The most important parameters and some resulting physical properties at 1 AU are given in Table 2.

4.1. Coronal Hole

In Figure 2a we show the velocity profiles for the main gas ions (protons and alpha particles) and for three test species, ^{3}He, ^{24}Mg, and ^{26}Mg. In Figure 2b the assumed

Table 2. Parameters of Solar Wind Models

Parameter	Streamer	Hole	Unit
$f_W(r_0)$	100	730	J m^{-2} s^{-1}
$B_r(r_0)$	5	27	10^{-4} T
Φ_α/Φ_e	0.01	0.04	
$n_e v_e$(1AU)	3.90	2.70	10^{12} m^{-2} s^{-1}
T_p(1AU)	0.35	2.50	10^5 K
T_e(1AU)	1.68	1.38	10^5 K
n_p(1AU)	11.50	3.30	10^6 m^{-3}
v_p(1AU)	332	750	km s^{-1}
B_r(1AU)	1.84	4.81	10^{-9} T

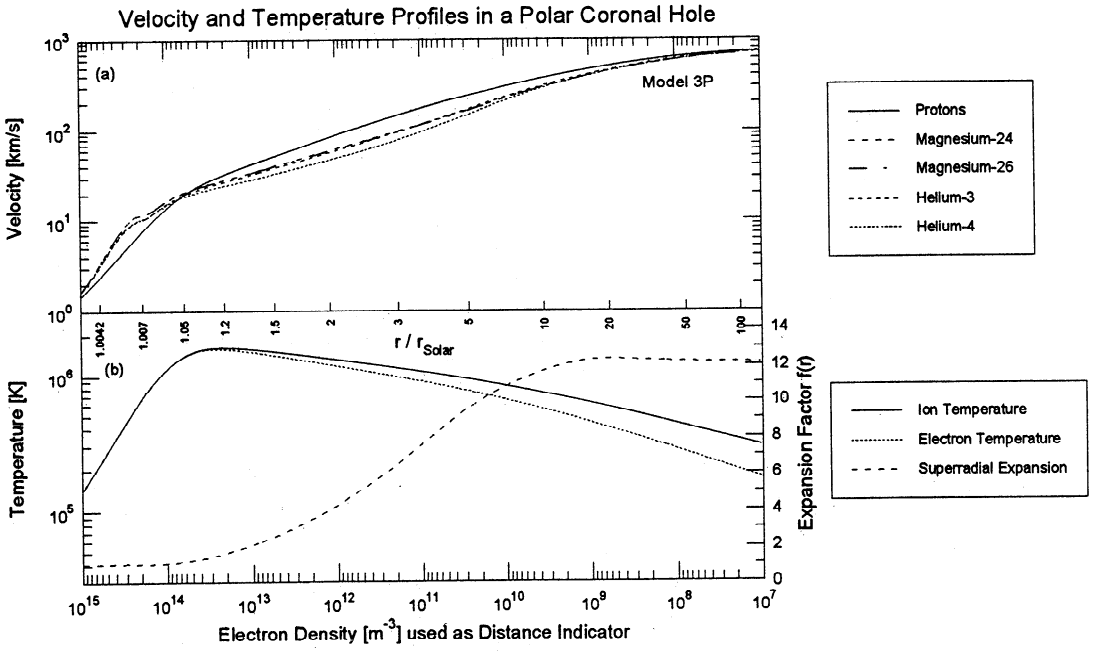

Figure 2. (a) Velocities in the fast solar wind are monotonically increasing with distance, reaching a common velocity of ~750 km s^{-1} at 1 AU. The electron density has been used as a distance scale. (b) The assumed temperature profiles and the superradial expansion factor are shown.

temperature profiles for ions and electrons and the superradial expansion factor are displayed. The electron density has been used as a distance scale in order to enlarge the region close to the Sun. The left end of the axis is in the upper part of the transition region; the right end is approximately at 0.6 AU (see heliospheric distances on central axis). The velocities in the fast solar wind are monotonically increasing with distance, reaching a common velocity of 750 km s^{-1} at 1 AU through acceleration by Alfvén waves. The velocity differences are relatively small in the whole acceleration region. This is caused by relatively strong coupling of

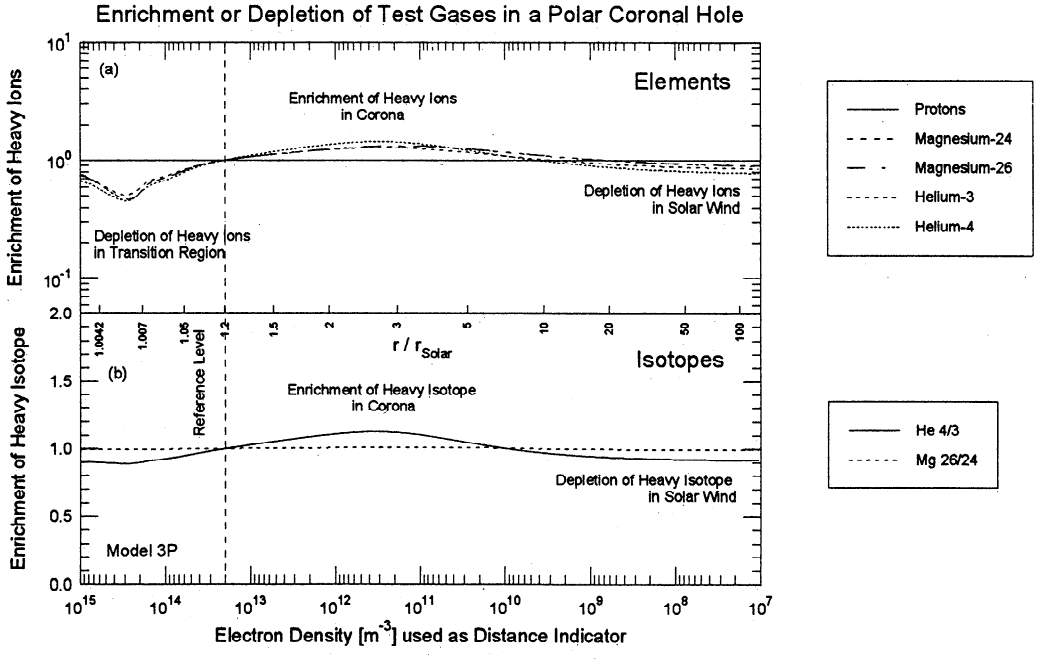

Figure 3. (a) The predicted enrichment of elements in a polar coronal hole is plotted. (b) The enrichment or depletion of the heavier isotope relative to the lighter one for helium and magnesium is shown. Both elemental and isotopic fractionation are very weak in the coronal hole associated solar wind.

the species by Coulomb friction and by the wave force. Heavy species usually flow somewhat slower than protons, approaching the proton speed at a few AU. In the transition region the situation is reversed: The thermal force, being proportional to the temperature gradient, accelerates heavy species relative to protons in the direction of the temperature maximum, leading to faster streaming of heavy ions. Since we have some doubts about the reality of the steep temperature gradient and the validity of a steady state description here, we use a reference level well above the transition region. We therefore make no attempt to explain the average helium depletion in the solar wind, which is probably caused by diffusion effects in the chromosphere [*Hansteen et al.*, 1993].

In Figure 3 we plot the abundance variations resulting from the differential speeds. Figure 3a illustrates the local enrichment of elements relative to protons, and Figure 3b shows the local enrichment or depletion of the heavier isotope relative to the lighter one. Figure 3 shows a slight enrichment of the heavier ions in the acceleration region above the reference level and a very weak depletion of the heavier species in the distant high-speed solar wind. Generally, the enrichment of species x relative to species y at location r normalized to the coronal reference location r_b is defined as

$$\text{enrichment}(x,y)(r) := \frac{\frac{n_x(r)}{n_y(r)}}{\frac{n_x(r_b)}{n_y(r_b)}} = \frac{\frac{v_y(r)}{v_x(r)}}{\frac{v_y(r_b)}{v_x(r_b)}}. \qquad (8)$$

It is useful to note that in the case of a solar wind with all species approaching the same asymptotic speed at large distances, the asymptotic enrichment factor is equal to the fractionation factor defined in (6) because density ratios are equal to the corresponding flux ratios in that case.

4.2. Coronal Streamer

The results of the model for the coronal streamer are displayed in the same way as for the coronal hole model. In Figure 4, velocities, temperatures, and the expansion factor are displayed. The flux tube expands rapidly between 1 and 2.5 solar radii, which leads, in the case of a constant integral flux Φ_p according to (4), to a reduced proton flux density $n_p v_p$ around the location of the maximum expansion factor. The correspondingly reduced Coulomb drag on the heavier species thus leads to their velocities being much slower than the proton speed [cf. *Bürgi*, 1992] in the rapidly expanding region. The particle velocities are no longer monotonically increasing with heliospheric distance. Note that alpha particles have the smallest speed, while ^{3}He and the much heavier Mg isotopes have speeds closer to the proton speed. This peculiar behavior is caused by the Coulomb friction and will be discussed in section 5.

In Figure 5 the elemental and isotopic enrichment factors according to the definition in (8) are plotted. The fractionation effect is very strong in the coronal streamer because the rapidly expanding geometry leads to big velocity differences between heavy particles and protons, as explained in the first paragraph of section 4.2.

In the corona above the reference level, all heavy elements are enriched compared to protons, while they are depleted in the solar wind. Our coronal streamer model represents an extreme case, with a ^{4}He/H ratio depressed by a factor 2.5 with respect to the reference level in the corona. Such large reductions of the ^{4}He/H ratio are consistent with observations in the slow solar wind close to the heliospheric current sheet [*Borrini et al.*, 1981]. This gives us some confidence in the results of our model. In the average interstream solar wind, however, the superradial expansion is probably not so violent, and the expected depression of ^{4}He/H is much smaller. This again is observed in the slow solar wind.

Figure 5b shows that heavy isotopes are enriched in the corona and depleted in the solar wind relative to lighter isotopes. The isotopic ratio ^{4}He/^{3}He in the slow solar wind is reduced by a factor of 1.5 compared to the reference location. Although we notice that the element magnesium is depleted in the solar wind relative to protons due to inefficient Coulomb friction, we find only a marginal fractionation of Mg isotopes. This result is consistent with magnesium isotopic ratios measured in the solar wind by *Bochsler et al.* [1996] and *Kucharek et al.* [1998].

The results for the element fractionation in the two analyzed solar wind regimes are summarized in Table 3. The fractionation factors for element abundances relative to hydrogen in the solar wind compared to the coronal reference level are calculated according to the definition in (6). All listed species are depleted in the solar wind relative to protons. The depletion is between 10 and 25% in our model for the fast solar wind, while the depletion in the slow solar wind is of the order of 40%. Usually ^{4}He is more strongly depleted than all other species. The results for the isotopic fractionation of some important isotope pairs in the solar wind are summarized in Table 4. Here again, the fractionation between two isotopes is calculated from the velocity ratios at the coronal reference level, according to (6). For the helium isotopic ratio fractionation factors between 0.69 and 0.92 indicate substantial fractionation effects, depending on the solar wind regime. For all other elements the depletion of a heavy isotope relative to a light isotope is of the order of only 2% per unit mass difference, even in our extreme model for a coronal streamer.

5. Influence of Coulomb Friction

In the lower corona, where the flow is well subsonic, the momentum equation for test particles can be simplified to a diffusion equation by calculating the difference between the test gas and the main gas acceleration [*Burgers*, 1969]. This is done here neglecting waves, rotational forces, and alpha particles in the main gas and

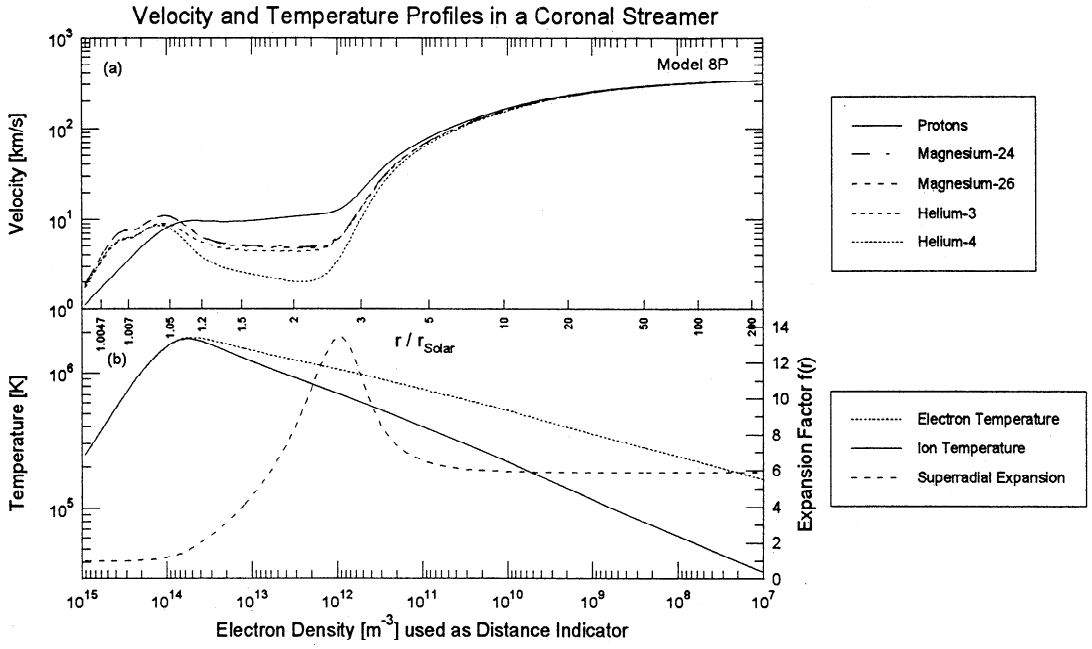

Figure 4. The coronal streamer geometry expands rapidly above the temperature maximum, which locally decreases the proton flux and reduces Coulomb friction between protons and heavier species. This retards heavier species and especially Helium-4.

assuming local thermal equilibrium (LTE) conditions [cf. *Geiss*, 1982]. The velocity v_x of a test gas with density n_x and temperature $T_x = T(r)$, consisting of particles with mass $m_x = A_x m_p$ and charge $Z_x e$ fulfills the following equation:

$$m_x \nu_{xp}(v_x - v_p) = -\frac{2A_x - Z_x - 1}{2}\frac{GMm_p}{r^2} - kT\frac{d\ln(n_x/n_p)}{dr} + k\alpha_x\frac{dT}{dr}, \quad (9)$$

where the Coulomb collision frequency ν_{xp} for the test particles with protons is given by

$$\nu_{xp} = \frac{16\sqrt{\pi}}{3}\left(\frac{Z_x e^2}{4\pi\epsilon_0}\right)^2 \ln\Lambda \frac{\sqrt{\mu_{xp}}}{(2kT_{xp})^{1.5}}\frac{n_p}{m_x}, \quad (10)$$

where

$$\mu_{xp} = m_x m_p/(m_x + m_p) \quad (11)$$

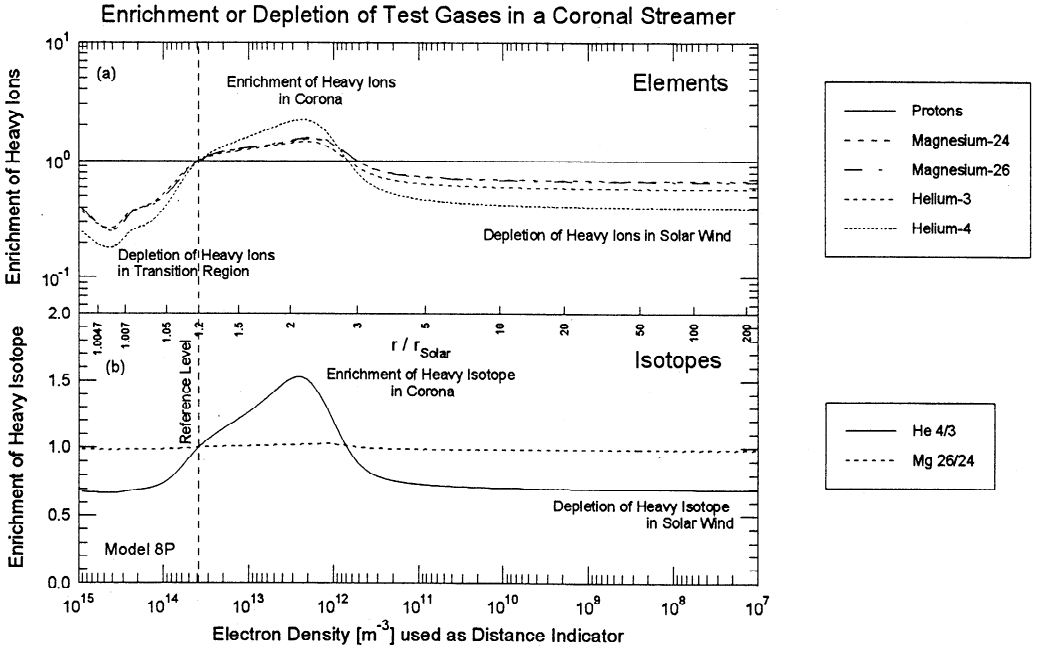

Figure 5. (a) Elemental fractionation relative to hydrogen is shown. ^{4}He shows the strongest depletion in the solar wind, while the effect on ^{3}He and the Mg isotopes is weaker. (b) Isotopic fractionation of helium and magnesium is illustrated. There is a noticeable effect on helium, while the fractionation between Mg isotopes is minor.

Table 3. Depletion of Heavy Elements in Solar Wind With Equal Ion Temperatures

Element Ratio	Coronal Streamer	Coronal Hole
^{3}He/H	0.57	0.83
^{4}He/H	0.40	0.76
^{12}C/H	0.64	0.84
^{14}N/H	0.62	0.83
^{16}O/H	0.61	0.84
^{20}Ne/H	0.64	0.86
^{24}Mg/H	0.67	0.87
^{28}Si/H	0.67	0.86
^{32}S/H	0.63	0.85

$$T_{xp} = (T_x m_p + T_p m_x)/(m_x + m_p) \quad (12)$$

denote the reduced mass and reduced temperature, respectively. In LTE, all species have the same temperature, and we find $T_{xp} = T_x = T_p$. The left-hand side of (9) shows the Coulomb friction with protons in the subsonic limit. The first term on the right-hand side is the gravitational force on the ions, which is reduced due to the influence of the radial electric field. The next term is the diffusion of test particles caused by the concentration gradient. The last term describes the thermal diffusion force which accelerates heavy particles toward higher temperatures. It is proportional to the temperature gradient with the species-dependent proportionality constant α_x.

If (9) is applied to a situation close to the temperature maximum where the temperature gradient vanishes and if the concentration gradient is neglected for the moment, the differential equation reduces to a simple explicit formula for the velocity of the test particles:

$$v_x = v_p \left(1 - \frac{H_x C_p f(r)}{\Phi_p}\right). \quad (13)$$

Here Φ_p is the proton flux as defined in (4) while the flux normalization constant C_p is defined as

$$C_p = \frac{GM}{2}\left(\frac{4\pi\epsilon_0}{e^2}\right)^2 \frac{(2kT_p)^{1.5}}{\ln\Lambda}\frac{3\sqrt{m_p}}{16\sqrt{\pi}}. \quad (14)$$

Equation (13) shows that for large proton fluxes, $\Phi_p \gg C_p$, the second term in the parenthesis vanishes and, as expected, the test particles move with the proton velocity. For smaller proton fluxes the test particles move slower. Furthermore it can be seen that the velocity difference increases with increasing superradial expansion factor $f(r)$ and with increasing temperature (via C_p). The numerical factor,

$$H_x = \frac{2A_x - Z_x - 1}{Z_x^2}\sqrt{\frac{A_x + 1}{A_x}}, \quad (15)$$

determines how strongly an ion with mass number A_x and charge number Z_x reacts on a reduced proton flux. Evidently, the values of H_x for different test particles define an ordering scheme for the velocities and thus for the expected fractionation factors. The lower limit of H_x is $H_p = 0$, the value for (unfractionated) protons. Alpha particles have an exceptionally large H_α=1.40, while ^{3}He^{2+} has a value of 0.87. For heavier ions such as O, Ne, Mg, Si, with the charge states prevailing in the corona, the factor H_x is between 0.5 and 0.9. This explains the close match of the magnesium velocities with the ^{3}He speed in Figures 2 and 4. The alpha particles always have the slowest flow speeds and will thus be accumulating in the corona relative to all other solar wind species. This is accompanied by a significant elemental and isotopic fractionation of helium.

6. Influence of Temperature

In our model the radial temperature profile for each species can be prescribed. In the first two cases, the ion temperature was chosen to be equal to the proton temperature everywhere. This would be the case in local thermal equilibrium, certainly fulfilled in the chromosphere and below. In the special case of the dense plasma along the heliospheric current sheet, observations often show similar temperatures for protons and alpha particles [*Borrini et al.*, 1981]. However, observations of ion temperatures in the solar wind usually reveal much higher temperatures for heavy ions than for protons [*Ogilvie et al.*, 1980; *Bochsler et al.*, 1985; *von Steiger et al.*, 1995]. Often the temperatures are proportional to the ion mass under the influence of wave particle interactions. Observation of Doppler-broadened widths of coronal emission lines by UVCS (Ultraviolet Coronograph Spectrometer) [*Kohl et al.*, 1997] and SUMER (Solar Ultraviolet Measurements of Emitted Radiation) [*Tu et al.*, 1998] on SOHO also gives evidence for high heavy ion temperatures already at low heights in the solar corona.

In order to discuss the influence of a mass-dependent temperature on the fractionation problem, we assume mass-proportional ion temperatures in the corona and solar wind. However, the ion temperatures in the chromosphere are equal to the proton and electron temperature due to frequent collisions. In the transition region the temperature profile is gradually switched from mass-independent to mass-proportional. This causes a mass-dependent temperature gradient.

Table 4. Depletion of Heavier Isotopes in Solar Wind With Equal Ion Temperatures

Isotope Ratio	Coronal Streamer	Coronal Hole
^{4}He/^{3}He	0.69	0.914
^{13}C/^{12}C	0.973	0.9888
^{15}N/^{14}N	0.975	0.9894
^{18}O/^{16}O	0.953	0.9834
^{22}Ne/^{20}Ne	0.972	0.9907
^{26}Mg/^{24}Mg	0.983	0.9937
^{30}Si/^{28}Si	0.986	0.9935
^{34}S/^{32}S	0.983	0.9935

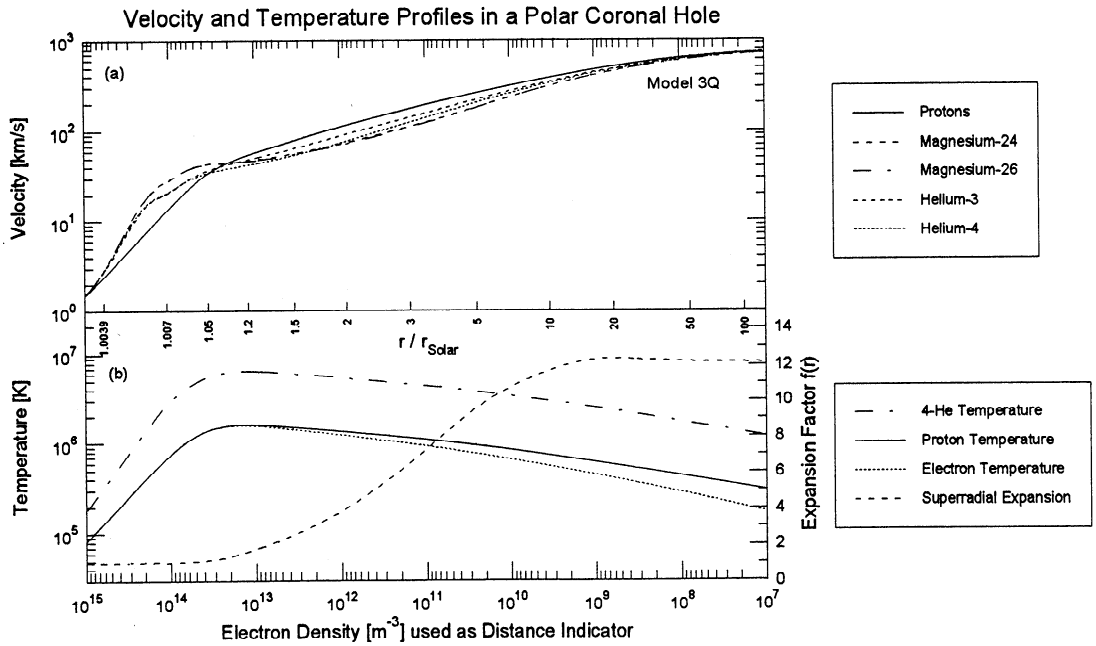

Figure 6. (a) Velocities in the fast solar wind are monotonically increasing with distance, reaching a common velocity of ~750 km s^{-1} at 1 AU. The electron density has been used as a distance scale. (b) The assumed mass-proportional temperatures and the superradial expansion factor are shown.

The assumption of mass-proportional temperatures for heavy ions in the corona increases the weighted temperature T_{xp} by up to a factor 2, if the proton temperature is maintained. This diminishes the Coulomb collision frequency and reduces the Coulomb drag. However, the thermal force, the result from heat flux interactions, is increased due to the increased temperature gradient in our model. However, the assumption of collisionally dominated flows, which is used to derive the heat fluxes from the temperature gradients, is less valid in the case of higher temperatures, and the precision of the results is worse. While the behavior of the third moment is questionable, it is evident that the assumption of mass-proportional temperatures for

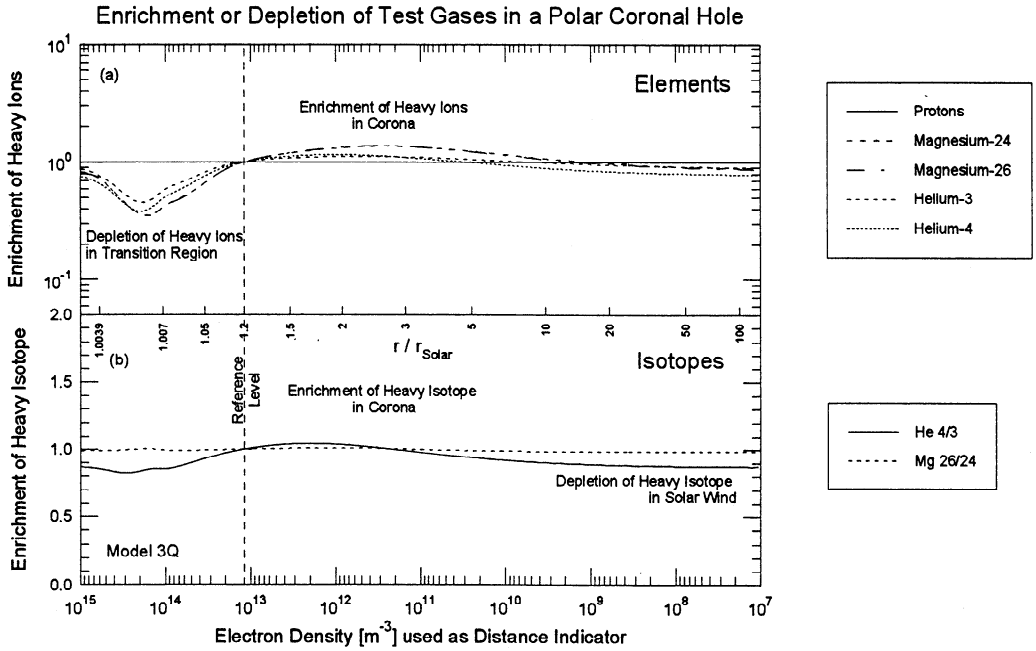

Figure 7. (a) The predicted enrichment of elements in a polar coronal hole is plotted. (b) The enrichment or depletion of the heavier isotope relative to the lighter one for helium and magnesium is shown. Both elemental and isotopic fractionation are very weak in the coronal hole associated solar wind.

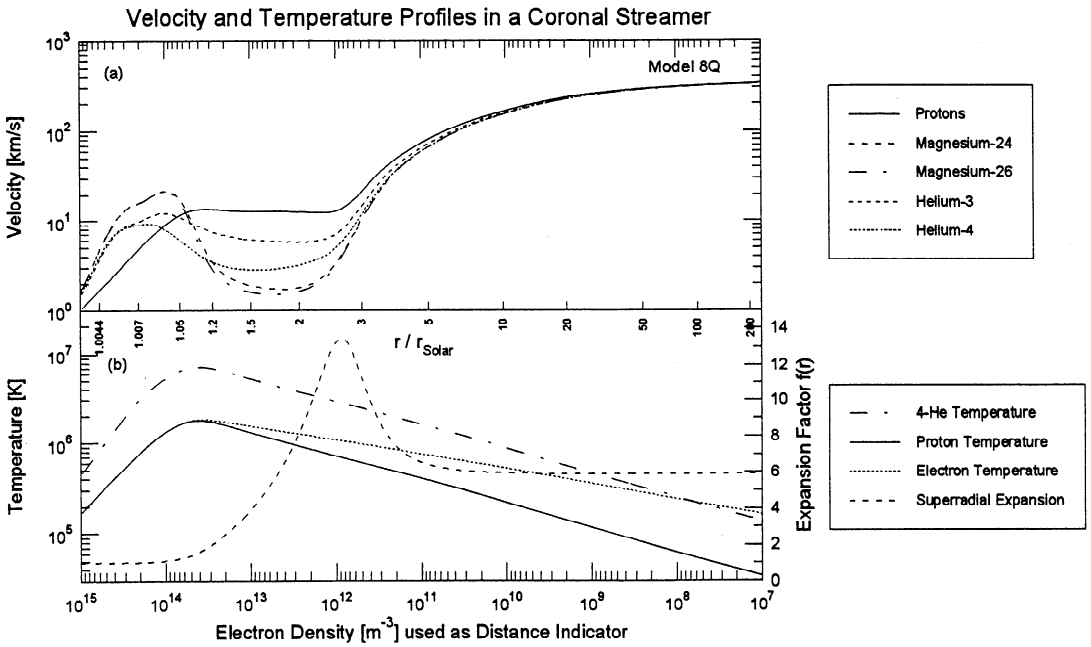

Figure 8. (a) Velocities in the slow solar wind are not monotonically increasing with distance. (b) The assumed mass-proportional temperature profiles and the superradial expansion factor are shown. This model is probably not realistic.

ions increases their pressure gradient, while gravity and electric field are not affected. This should lead to a better acceleration of heavy ions in the solar wind, even without friction, and the fractionation with respect to hydrogen should be reduced. The two cases have been recalculated for mass-proportional temperatures. The mass-proportional temperatures and velocities for the fast solar wind are shown in Figure 6. The corresponding elemental and isotopic enrichment factors are given in Figure 7. The results for the coronal streamer are displayed in Figures 8 and 9. The resulting element fractionation is tabulated in Table 5, and the isotopic fractionation is given in Table 6. In the high-speed solar wind the results are similar to the case with equal temperatures. The elemental fractionation effect is between 10 and 25% for all ions, the isotope effect is of the order of 3% for heavy ions.

In the coronal streamer model, surprisingly the frac-

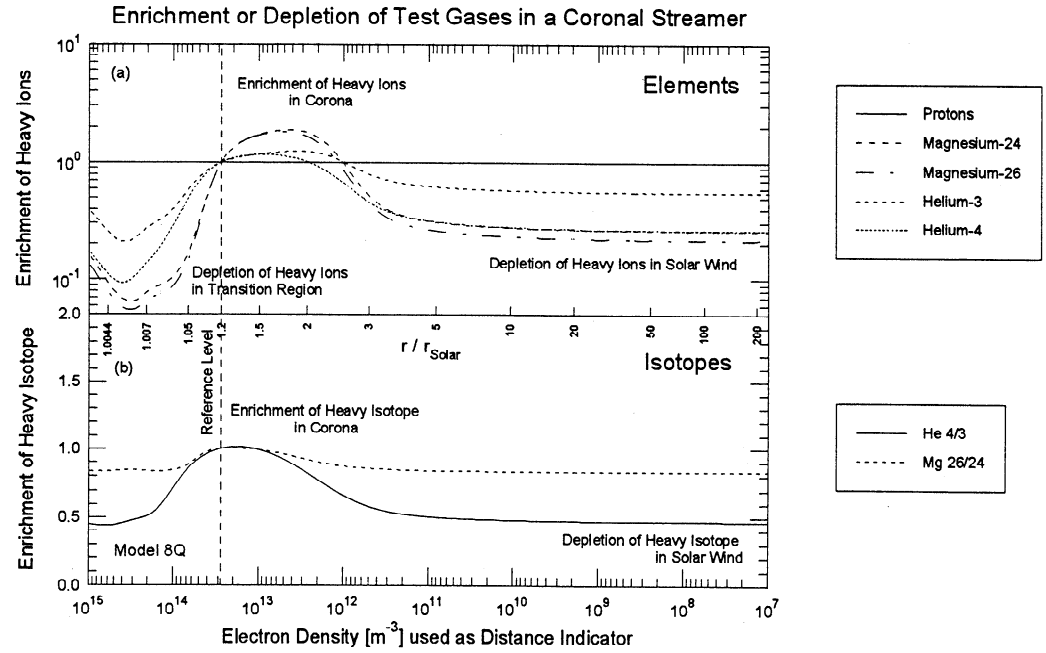

Figure 9. The depletion of heavy elements and isotopes in the slow solar wind with mass-proportional temperatures is unrealistically strong.

Table 5. Depletion of Heavy Elements in Solar Wind With Mass-Proportional Ion Temperatures

Element Ratio	Coronal Streamer	Coronal Hole
^{3}He/H	0.55	0.89
^{4}He/H	0.26	0.77
^{12}C/H	0.28	0.80
^{14}N/H	0.21	0.79
^{16}O/H	0.17	0.82
^{20}Ne/H	0.21	0.86
^{24}Mg/H	0.26	0.86
^{28}Si/H	0.19	0.84
^{32}S/H	0.10	0.81

tionation is not reduced by the assumption of mass-proportional temperatures. On the contrary, the heavy species flow even slower in the region of strong superradial expansion than in the isothermal model. A close inspection of the force balance of heavy species shows that the pressure gradient is, indeed, much stronger than before. However, it is still not large enough to accelerate the heavy ions with the same rate as the protons. This is due to the fact that in addition to the partial pressure, the influence of the electric field is important for charged particles. As the charge/mass ratio is higher for protons, than for heavy species, protons are still favored. In our model the deficit in accelerating forces can only be compensated by Coulomb friction. As the collision frequency is reduced, a larger velocity difference is necessary to provide the needed frictional force. This is the cause for the substantial fractionation effect. The depletion of He/H by almost a factor of 4 is extreme and rarely observed in coronal streamers. However, the theoretical consideration does not take acceleration of minor species induced by wave dissipation into account and is therefore not self-consistent. Indeed, the appearance of mass proportionality in kinetic temperatures of minor species requires strong wave particle interaction which would undoubtedly lead to acceleration of these species thus diminishing the fractionation effect.

If the analysis from section 5 is generalized to the case of species-dependent temperatures (T_x, T_p, T_e), we find a generalized ordering parameter H_x for inclusion in (13):

$$H_x = \frac{2[A_x(T_p+T_e) - T_x - Z_x T_e](A_x + T_x/T_p)^{1.5}}{Z_x^2(T_p+T_e)\sqrt{A_x}(A_x+1)}, \tag{16}$$

while the remaining factor, $C_p f(r)/\Phi_p$, is not modified. In the case of mass-proportional temperatures $T_x = A_x T_p$ for ions, two large terms inside the bracket in the numerator cancel, and we get

$$H_x = \frac{A_x - Z_x}{Z_x^2}\left(\frac{2^{1.5}A_x}{A_x+1}\right)\frac{2T_e}{T_p+T_e}. \tag{17}$$

This formula shows that the finite electron temperature and thus the electric field are responsible for the residual fractionation. As all ions except protons have mass/charge ratios exceeding unity, the factor H_x is positive, and all species will lag behind protons. Here also, alpha particles tend to be affected more strongly than heavier ions. However, the dependence of H_x on the actual charge state is more pronounced than in the isothermal case. These findings help in understanding the strong fractionation in the, probably unrealistic, mass-proportional temperature case for a rapidly expanding coronal streamer flux tube geometry. If the results of this model were true, substantial isotopic fractionations of the order of 20% should be observed in the solar wind close to heliospheric current sheets. To our knowledge no such events have been reported yet. Furthermore, heavy elements such as oxygen and sulfur should be depleted relative to alpha particles in these regions. Observations made by *Wimmer* [1994] show a slight reduction of the He/O ratio in the solar wind close to the current sheet, which is consistent with the isothermal model but in contradiction to the present model. We therefore reject the model with mass-proportional temperatures for the coronal streamer, while the model for the coronal hole does not depend much on the assumption about the temperatures. The model with mass-independent temperatures seems to be more realistic for the case of the heliospheric current sheet. This view is supported by observations of *Borrini et al.* [1981] and by recent observations of kinetic temperatures of minor ions in the solar wind at 1 AU by *Hefti et al.* [1998].

7. Conclusions

We have modeled the solar wind acceleration region and determined elemental and isotopic fractionation between a reference point in the corona and the distant solar wind. The model for high-speed solar wind from a polar coronal hole shows a depletion of heavy ions in the solar wind of 10-25%, while the model for a coronal streamer with extreme superradial expansion yields stronger depletions of heavy particles (up to a factor 2.5 for He/H). The fractionation pattern is mainly determined by the efficiency of Coulomb friction with protons in the acceleration region of the so-

Table 6. Depletion of Heavier Isotopes in Solar Wind With Mass-Proportional Ion Temperatures

Isotope Ratio	Coronal Streamer	Coronal Hole
^{4}He/^{3}He	0.47	0.871
^{13}C/^{12}C	0.81	0.970
^{15}N/^{14}N	0.81	0.972
^{18}O/^{16}O	0.67	0.960
^{22}Ne/^{20}Ne	0.77	0.979
^{26}Mg/^{24}Mg	0.83	0.984
^{30}Si/^{28}Si	0.80	0.983
^{34}S/^{32}S	0.80	0.983

lar wind. The approximate ordering parameter for the fractionation of different species relative to protons is $[(A_x+1)/A_x]^{1/2}(2A_x-Z_x-1)/Z_x^2$ which is largest for alpha particles and vanishes for protons. This causes a large reduction of the ^{4}He/H ratio in the solar wind close to a heliospheric current sheet, while the average slow solar wind is less affected. Such a variability of the alpha/proton ratio in the solar wind is indeed observed. The isotopic fractionation of helium can amount to 30% in extreme cases while the effect on the isotopic ratios of heavier species is usually <3% per unit mass difference.

For the case of fast solar wind from a coronal hole, we find no big change in the fractionation pattern, if mass-proportional temperatures are assumed instead of equal ion temperatures. We also tried to make a model of a coronal streamer with mass-proportional temperatures. However, this is not a realistic assumption for such a collisionally dominated flow, and indeed, the resulting fractionation is not consistent with in situ observations. A first comparison of the results of our model with solar wind composition data was provided by *Bodmer and Bochsler* [1998]. Further comparisons will show how precise the predictions are. Of course there is room for improvement of the model, e.g., by including equations for pressure tensors and heat fluxes, by more realistic treatment of wave particle interactions and coronal heating, or by extending the model to the lower solar atmosphere. However, since our model reproduces the observed variability of the FIP-independent part of the elemental fractionation in the correct order of magnitude, we conclude that it is suitable to predict the orders of magnitude for the most significant effects on isotopes in the solar wind.

Acknowledgments. This work was supported by the Swiss National Science Foundation and by the Max-Planck Society (Germany).

Michel Blanc thanks Viviane Pierrard and another referee for their assistance in evaluating this paper.

References

Anders, E., and N. Grevesse, Abundances of the elements: Meteoritic and solar, *Geochim. Cosmochim. Acta*, *53*, 197–214, 1989.

Arnaud, M., and R. Rothenflug, An updated evaluation of recombination and ionization rates, *Astron. Astrophys. Suppl. Ser.*, *60*, 425–457, 1985.

Bame, S. J., A. J. Hundhausen, J. R. Asbridge, and I. B. Strong, Solar wind ion composition, *Phys. Rev. Lett.*, *20*, 393–395, 1968.

Bochsler, P., J. Geiss, and R. Joos, Kinetic temperatures of heavy ions in the solar wind, *J. Geophys. Res.*, *90*, 10,779–10,789, 1985.

Bochsler, P., M. Gonin, R. B. Sheldon, T. Zurbuchen, G. Gloeckler, D. C. Hamilton, M. R. Collier, and D. Hovestadt, Abundance of solar wind magnesium isotopes determined with WIND/MASS, in *Proceedings of the Eighth International Solar Wind Conference*, edited by D. Winterhalter et al., vol. 382 of *AIP Conf. Proc.*, pp. 199–202, 1996.

Bodmer, R., The helium isotopic ratio as a test for minor ion fractionation in the solar wind acceleration process: SWICS/ULYSSES data compared with results from a multifluid model, Ph.D. thesis, Univ. of Bern, Bern, Switzerland, 1996.

Bodmer, R., and P. Bochsler, The helium isotopic ratio in the solar wind and ion fractionation in the corona by inefficient coulomb drag, *Astron. Astrophys.*, *337*, 921–927, 1998.

Borrini, G., J. T. Gosling, S. J. Bame, W. C. Feldman, and J. M. Wilcox, Solar wind helium and hydrogen structure near the heliospheric current sheet: A signal of coronal streamers at 1 AU, *J. Geophys. Res*, *86*, 4565–4573, 1981.

Burgers, J. M., *Flow Equations for Composite Gases*, Academic, San Diego, Calif., 1969.

Bürgi, A., Dynamics of alpha particles in coronal streamer type geometries, in *Solar Wind Seven*, pp. 333–336, Pergamon Press, Tarrytown, N.Y., 1992.

Bürgi, A., and J. Geiss, Helium and minor ions in the corona and solar wind: Dynamics and charge states, *Sol. Phys.*, *103*, 347–383, 1986.

Coplan, M. A., K. W. Ogilvie, P. Bochsler, and J. Geiss, Interpretation of ^{3}He abundance variations in the solar wind, *Sol. Phys.*, *93*, 415–434, 1984.

Gabriel, A. H., A magnetic model of the solar transition region, *Philos. Trans. R. Soc. London A*, *281*, 339–352, 1976.

Geiss, J., Processes affecting abundances in the solar wind, *Space Sci. Rev.*, *33*, 201–217, 1982.

Geiss, J., P. Hirt, and H. Leutwyler, On acceleration and motion of ions in corona and solar wind, *Sol. Phys.*, *12*, 458–483, 1970.

Geiss, J., F. Bühler, H. Cerutti, P. Eberhardt, and C. Filleux, Solar-wind composition experiment, in *Apollo 16 Preliminary Science Report*, vol. 315, pp. 14.1–14.10, NASA Spec. Publ., 1972.

Gloeckler, G., et al., The solar wind ion composition spectrometer, *Astron. Astrophys. Suppl. Ser.*, *92*, 267–289, 1992.

Gloeckler, G., et al., The solar wind and suprathermal ion composition investigation on the WIND spacecraft, *Space Sci. Rev.*, *71*, 79–124, 1995.

Gloeckler, G., J. Cain, F. M. Ipavich, E. O. Tums, P. Bedini, R. F. Wimmer-Schweingruber, J. Geiss, and R. Kallenbach, Investigation of the composition of solar and interstellar matter using solar wind and pickup ion measurements with SWICS and SWIMS on the ACE spacecraft, *Space Sci. Rev.*, *86*, 497–539, 1998.

Hansteen, V. H., and E. Leer, Coronal heating, densities, and temperatures and solar wind acceleration, *J. Geophys. Res.*, *100*, 21,577–21,593, 1995.

Hansteen, V. H., T. E. Holzer, and E. Leer, Diffusion effects on the helium abundance of the solar transition region and corona, *Astrophys. J.*, *402*, 334–343, 1993.

Hansteen, V. H., E. Leer, and T. E. Holzer, The role of helium in the outer solar atmosphere, *Astrophys. J.*, *482*, 498–509, 1997.

Hefti, S., et al., Kinetic properties of solar wind minor ions and protons measured with SOHO/CELIAS, *J. Geophys. Res.*, *103*, 29,697–29,704, 1998.

Hovestadt, D., et al., CELIAS - Charge, element and isotope analysis system for SOHO, *Sol. Phys.*, *162*, 441–481, 1995.

Hu, Y. Q., R. Esser, and S. R. Habbal, A fast solar wind model with anisotropic proton temperature, *J. Geophys. Res*, *102*, 14,661–15,676, 1997.

Isenberg, P. A., and J. V. Hollweg, Finite amplitude Alfvén waves in a multi-ion plasma: Propagation, acceleration, and heating, *J. Geophys. Res.*, *87*, 5023–5029, 1982.

Kohl, J. L., G. Noci, E. Antonucci, and G. Tondello, First results from the SOHO Ultraviolet Coronograph Spectrometer, *Sol. Phys.*, *175*, 613–644, 1997.

Kucharek, H., et al., Magnesium isotopic composition as

observed with the CELIAS/MTOF experiment on the SOHO spacecraft, *J. Geophys. Res*, *103*, 26,805–26,812, 1998.

Leblanc, F., and D. Hubert, A generalized model for the proton expansion in astrophysical winds, I.; The velocity distribution function representation, *Astrophys. J*, *483*, 464–474, 1997.

Marsch, E., Kinetic physics of the solar wind plasma, in *Physics of the Inner Heliosphere II*, edited by R. Schwenn and E. Marsch, pp. 45–133, Springer-Verlag, New York, 1991.

Marsch, E., R. von Steiger, and P. Bochsler, Element fractionation by diffusion in the solar chromosphere, *Astron. Astrophys*, *301*, 261–276, 1995.

McKenzie, J. F., W. H. Ip, and W. I. Axford, The acceleration of minor ion species in the solar wind, *Astrophys. Space Sci.*, *64*, 183–211, 1979.

Meyer, J.-P., The baseline composition of solar energetic particles, *Astrophys. J. Suppl. Ser.*, *57*, 151–171, 1985.

Ogilvie, K. W., P. Bochsler, J. Geiss, and M. A. Coplan, Observations of the velocity distribution of solar wind ions, *J. Geophys. Res*, *85*, 6069–6074, 1980.

Olsen, E. L., E. Leer, and O. Lie-Svendsen, An eight-moment model parameter study of the solar wind: dependence on variations in coronal heating, *Astron. Astrophys.*, *338*, 747–755, 1998.

Peter, H., Velocity-dependent fractionation in the solar chromosphere, *Astron. Astrophys.*, *312*, L37–L40, 1996.

St.-Maurice, R.-P., and R. W. Schunk, Diffusion and heat flow equations for the mid-latitude topside ionosphere, *Planet. Space Sci.*, *25*, 907–920, 1976.

Tu, C.-Y., E. Marsch, K. Wilhelm, and W. Curdt, Ion temperatures in a solar polar coronal hole observed by SUMER on SOHO, *Astrophys. J.*, *503*, 475–482, 1998.

von Steiger, R., and J. Geiss, Supply of fractionated gases to the corona, *Astron. Astrophys.*, *225*, 222–238, 1989.

von Steiger, R., J. Geiss, G. Gloeckler, and A. B. Galvin, Kinetic properties of heavy ions in the solar wind from SWICS/ULYSSES, *Space Sci. Rev.*, *72*, 71–76, 1995.

Wang, Y.-M., and N. R. Sheeley Jr., Solar wind speed and coronal flux-tube expansion, *Astrophys. J.*, *355*, 726–732, 1990.

Wimmer, R. F., Oxygen, helium, and hydrogen in the solar wind: SWICS/ULYSSES results, Ph.D. thesis, Univ. of Bern, Bern, Switzerland, 1994.

R. Bodmer, P. Bochsler, Physikalisches Institut, Universität Bern, Sidlerstrasse 5, CH-3012 Bern, Switzerland (bodmer@linmpi.mpg.de, bochsler@soho.unibe.ch)

(Received September 3, 1998; revised June 4, 1999; accepted July 15, 1999.)